PHYSICAL REVIEW A **96**, 041401(R) (2017)

Alignment-dependent population inversion in N_2^+ in intense few-cycle laser fields

Huailiang Xu,[1,2,3] Erik Lötstedt,[1] Toshiaki Ando,[1] Atsushi Iwasaki,[1] and Kaoru Yamanouchi[1,*]
[1]*Department of Chemistry, School of Science, The University of Tokyo, 7-3-1 Hongo, Bunkyo-ku, Tokyo 113-0033, Japan*
[2]*State Key Laboratory of Precision Spectroscopy, East China Normal University, Shanghai 200062, China*
[3]*State Key Laboratory on Integrated Optoelectronics, College of Electronic Science and Engineering, Jilin University, Changchun 130012, China*

(Received 12 May 2017; published 19 October 2017)

We align nonadiabatically an ensemble of N_2 in air, and irradiate the ensemble with linearly polarized intense few-cycle laser pulses to generate population-inverted N_2^+ ions. By probing the self-seeded lasing signals of N_2^+ at 391 nm, we show that the ultrafast population inversion in N_2^+ between the electronic ground $X\,^2\Sigma_g^+$ state and the electronically excited $B\,^2\Sigma_u^+$ state is sensitively influenced by the extent of the alignment of N_2 with respect to the polarization direction of the few-cycle laser field. The observed alignment dependence of the air lasing is reproduced well by numerical calculations performed based on a theoretical model in which the population transfer to the $B\,^2\Sigma_u^+$ state from the $X\,^2\Sigma_g^+$ state of N_2^+ in the ultrashort laser field is mediated by the $A\,^2\Pi_u$ state. Our findings show that the intensity of the air lasing can be manipulated precisely by the timing between the laser pulses inducing the alignment of N_2 and the laser pulse ionizing N_2 into N_2^+ as well as by the difference in the laser polarization directions of these laser pulses.

DOI: 10.1103/PhysRevA.96.041401

Population inversion in a gaseous medium induced by intense laser pulses is an attractive phenomenon in view of its potential applicability to mirrorless lasers in air, which can be a coherent and unidirectional light source for stand-off spectroscopy and remote sensing [1–6]. So far, it has been demonstrated that both of the two major atmospheric molecular species, i.e., nitrogen and oxygen molecules, can be population inverted by intense laser pulses, giving rise to forward or backward coherent emissions [7–14]. In particular, it was recently reported that the electronically excited $B\,^2\Sigma_u^+$ state of N_2^+ can be more populated in intense laser fields than the electronic ground $X\,^2\Sigma_g^+$ state, resulting in coherent narrow-band emissions from several vibrational levels in the $B\,^2\Sigma_u^+$ state to the vibrational levels in the $X\,^2\Sigma_g^+$ states [7]. It was demonstrated that the coherent N_2^+ emissions can be enhanced by a pulse train modulated by adaptive optics [15]. Most recently, it was revealed that the population-inverted N_2^+ can be created by few-cycle laser pulses within few femtoseconds [12]. A few scenarios such as field-induced multiple recollisions [16] and post-ionization multiple state coupling [12,17] have been proposed as possible mechanisms of the ultrafast formation of population-inverted N_2^+. If the mechanism is clarified, optimal conditions for achieving efficient air lasing can be explored, and consequently, a variety of applications of air lasing for nonlinear optics [18] and remote sensing [13,14] will be developed.

In the previous studies on air lasing modulated by the rotational coherence of N_2^+ [11,13,15], three different excitation processes, that is, the alignment of N_2, its ionization into N_2^+, and the creation of the inverted population between the $X\,^2\Sigma_g^+$ and $B\,^2\Sigma_u^+$ states in N_2^+, were achieved within the same laser pulse whose pulse durations are in the range of 30–200 fs. In the present study, in order to extract the effect of molecular alignment in air lasing, we first align N_2 nonadiabatically by irradiating air with a relatively weak femtosecond (∼50 fs) laser pulse, and then, after a certain delay time, we irradiate the ensemble of nonadiabatically aligned N_2 with an intense few-cycle laser pulse, which generates population-inverted N_2^+ serving as the gain medium and the white-light continuum serving as the seed.

Hereafter, we will call the weaker pump laser pulse the alignment pulse and the stronger probe laser pulse the ionization pulse, and denote the delay time between the ionization laser pulse with respect to the alignment laser pulse as τ. We record the intensity of the air lasing at 391 nm by varying systematically the delay time τ and the angle α between the polarization direction of the alignment pulse and that of the ionization pulse. We also perform numerical simulations based on the "post-ionization three-state coupling" scheme we proposed [12] for the creation of the inverted population, and compare the results with the observed signals.

We split a linearly polarized output of a femtosecond Ti:sapphire laser system (5 kHz, 800 nm, 30 fs, 500 μJ) into two. One is used for generating a weak alignment pulse (chirped to ∼50 fs, 34 μJ) with which we align N_2 in air. The other is used for generating an intense few-cycle ionization pulse [∼6.3 fs (FWHM), 49 μJ] by hollow-core fiber compression followed by chirp-mirror compression.

We propagate the compressed ionization pulse and focus it by a parabolic mirror ($f = 7.5$ cm) into the nonadiabatically aligned N_2 sample gas to form a short plasma channel whose length is 2–3 mm. The light field intensity achieved by the present tight focusing conditions is estimated to be $\sim 4.3 \times 10^{15}$ W/cm^2 when a Gaussian spatial distribution is assumed for the few-cycle laser pulse and the plasma defocusing effect is neglected. It has been known that the light field intensity could be one order of magnitude smaller by the plasma defocusing effect [12]. Therefore, the light field intensity of $\sim 4.3 \times 10^{15}$ W/cm^2 can be regarded as an upper limit of the light field intensity at the focus. We collimate the forwardly propagating light by a concave mirror ($f = 10$ cm), and then, focus the beam by a lens ($f = 14$ cm) and record the spectrum by a fiber spectrometer [19].

*kaoru@chem.s.u-tokyo.ac.jp

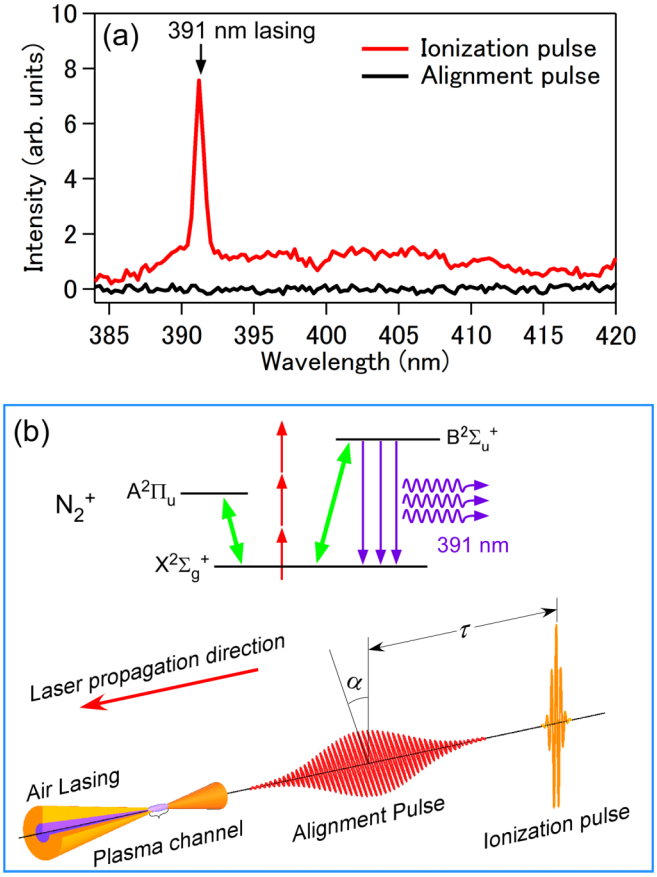

FIG. 1. (a) Forward spectrum obtained with the alignment pulses only (black solid line) and that obtained with the ionization pulses only (red solid line). (b) Schematic diagram for the generation of the 391-nm laser through the post-ionization optical coupling (green double-headed arrows) of the ensemble of nonadiabatically aligned N_2 induced by the alignment pulse after the ionization (red up arrows) by the ionization pulse.

In the spectrum of the forward emission induced only by the ionization laser pulses, we observed two sharp emission lines at 391 and 428 nm embedded on the tail part of the strong emission profile peaked at 800 nm, originating from the self-phase modulation in air. The emission lines at 391 and 428 nm can be assigned respectively to the self-seeded lasing at the $B\,^2\Sigma_u^+(v'=0)$-$X\,^2\Sigma_g^+(v=0)$ and $B\,^2\Sigma_u^+(v'=0)$-$X\,^2\Sigma_g^+(v=1)$ emissions as have been assigned in the previous reports [7–10].

In Fig. 1(a), we show the forward spectrum (red solid line) in the wavelength region between 383.5 and 420 nm. The lasing emission at 391 nm shows that the population inversion is achieved in N_2^+ between the $B\,^2\Sigma_u^+(v'=0)$ state and the $X\,^2\Sigma_g^+(v=0)$ state. The strong white light results from the self-phase modulation of the ionization pulse during the propagation in air, in which the high intensity of the ionization pulse ionizes air molecules and induces the change in the refractive index of air in the plasma, leading to a broad frequency distribution.

It is confirmed that the lasing at 391 nm does not occur only by the alignment pulses as shown in Fig. 1(a). The lasing in air at 391 nm produced by the ionization pulses can be ascribed to the amplification of the $B\,^2\Sigma_u^+$-$X\,^2\Sigma_g^+$ emission by the white light [12]. As shown in Fig. 1(b), the population inversion of N_2^+ is achieved first through the $A\,^2\Pi_u$-$X\,^2\Sigma_g^+$ and $B\,^2\Sigma_u^+$-$X\,^2\Sigma_g^+$ electronic state couplings in N_2^+ produced in an earlier part of the intense few-cycle laser pulse, and then, the $B\,^2\Sigma_u^+(v'=0)$-$X\,^2\Sigma_g^+(v=0)$ emission is amplified by the broad band white light whose spectrum covers the $B\,^2\Sigma_u^+(v'=0)$-$X\,^2\Sigma_g^+(v=0)$ transition.

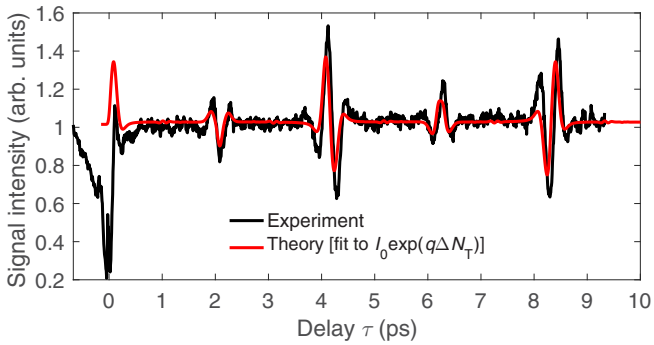

FIG. 2. Black solid line: Recorded intensity of the 391-nm lasing signal as a function of the delay time τ between the alignment pulse and the ionization pulse. Red solid line: Theoretical lasing signal $I_{\text{lasing}} = I_0 e^{q\Delta N_T}$, where q and I_0 are fitting parameters.

In Fig. 2, we show the recorded intensity of the 391-nm lasing signal as a function of τ. In the measurements, we set the angle α to be zero ($\alpha = 0$). It can be seen in this figure that the 391-nm laser signal has a strong dependence on τ, reflecting the revival of a rotational wave packet of N_2 created by the alignment pulse. For example, the lasing signal intensity becomes maximum at the half revival time, 4.1 ps, when N_2 molecules are aligned along the laser polarization direction, and it becomes minimum at 4.2 ps when they are antialigned, showing the strong dependence of the lasing emissions on the rotational coherence of N_2 molecules. Indeed, by simply adjusting the delay time τ within a very short time range of the order of 0.1 ps, we can enhance or suppress the 391-nm lasing signal.

Then, by fixing τ at $\tau = 4.1$ ps, we rotate the polarization direction of the alignment pulse so that the angle α increases by inserting a half-wave plate into the optical path for the alignment pulse, and record the intensity of the lasing at 391 nm. As shown in Fig. 3, the lasing intensity exhibits a

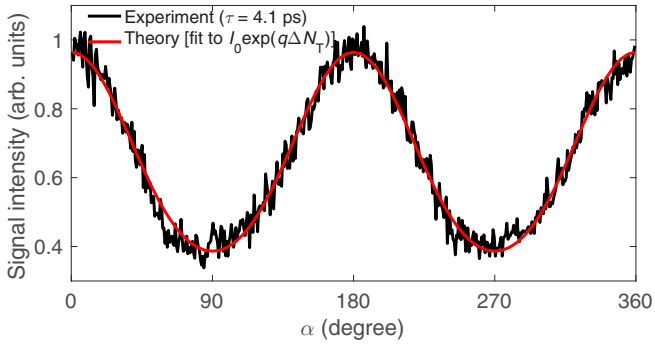

FIG. 3. Black solid line: Recorded intensity of the 391-nm lasing signal as a function of the angle α. Red solid line: Theoretical lasing signal $I_{\text{lasing}} = I_0 e^{q\Delta N_T}$ with $\Delta N_T(\tau = 4.1\text{ ps}, \alpha)$.

sinusoidal variation so that it becomes maximum when the N-N molecular axis is parallel to the polarization direction of the ionization pulse ($\alpha = 0$), and becomes minimum when the N-N molecular axis is perpendicular to the polarization direction of the ionization pulse ($\alpha = \pi/2$), showing that the lasing is sensitively dependent on the angle α.

It has been known that a refractive index of a gaseous sample is changed when molecules in the ensemble are aligned, and therefore, the refractive index change can influence the propagation direction of femtosecond laser pulses [20–23]. Because we propagate both of the alignment and ionization laser pulses coaxially, the deflection of the propagation direction of the femtosecond laser pulses could not be induced in our experimental setup. Furthermore, only rotational revivals of N_2 molecules can be seen in Fig. 2, that is, no revival structures of O_2 molecules can be identified, which means that the τ dependence of the 391-nm lasing signal cannot be explained by the refractive index change induced by the molecular alignment.

In order to understand the mechanism of the alignment-dependent lasing phenomena recorded in Figs. 2 and 3, we extend our theoretical model for air lasing [12], in which the light-field-induced coupling in N_2^+ between the $X\,^2\Sigma_g^+$ state and the $A\,^2\Pi_u$ state and that between the $X\,^2\Sigma_g^+$ state and the $B\,^2\Sigma_u^+$ state are taken into account, by combining this model with the time-dependent rotational motion of N_2 induced by an alignment laser pulse.

As a first step, we solve the rigid-rotor time-dependent Schrödinger equation (TDSE) for the rotational motion of N_2 induced by the alignment pulse [24],

$$i\hbar\frac{\partial\psi(\vartheta,\varphi,t)}{\partial t} = \left[H_{\rm rot} - \frac{1}{4}\Delta\alpha F^2(t)\cos^2\vartheta\right]\psi(\vartheta,\varphi,t), \quad (1)$$

where the angle ϑ denotes the angle between the N-N molecular axis and the polarization direction of the alignment laser pulse, φ the azimuthal angle, $H_{\rm rot}$ the field-free rigid-rotor Hamiltonian, $\Delta\alpha \approx 0.68$ Å^3 [25] the anisotropy of the polarizability, and $F(t)$ the field envelope of the alignment pulse whose Gaussian amplitude becomes maximum at $t = 0$. Equation (1) is solved by expanding the wave packet by field-free rotational eigenstates as

$$\psi(\vartheta,\varphi,t) = \frac{e^{iM\varphi}}{\sqrt{2\pi}}\sum_{j=0}^{J_{\rm max}} C_j^{JM}(t)P_j^M(\vartheta), \quad (2)$$

where $P_j^M(\vartheta)$ is a normalized associated Legendre function, and $J_{\rm max} = 30$. The values of the coefficients $C_j^{JM}(t)$ are obtained numerically with the initial rotational eigenstate $|J,M\rangle$, i.e., $C_j^{JM}(t = -T_0) = \delta_{jJ}$. After the rotational excitation by the alignment laser pulse, the thermally averaged rotational distribution of N_2,

$$D(\vartheta;\tau) = K^{-1}\sum_{J=0}^{J_{\rm max}} g_J e^{-(BJ(J+1)/k_BT)} \times \sum_{M=-J}^{J}\left|\sum_j C_j^{JM}(\tau)P_j^M(\vartheta)\right|^2, \quad (3)$$

is created as a function of the delay time τ, where $\tau = 0$ is defined as the time when the alignment pulse $F(t)$ takes its maximum value. In Eq. (3), g_J represents the statistical weight of the rotational level J with $g_J = 2$ for even J and $g_J = 1$ for odd J, K represents the normalization factor, $K = \sum_J g_J(2J+1)e^{-(BJ(J+1)/k_BT)}$, T the temperature, k_B the Boltzmann constant, and B the rotational constant of $^{14}N_2$ whose value is $B = 1.9895$ cm^{-1} [26].

At a given fixed angle α, we obtain the rotational distribution $U(\theta,\phi;\tau,\alpha)$ as

$$U(\theta,\phi;\tau,\alpha) = D(\vartheta;\tau), \quad (4)$$

where θ is the angle between the N-N molecular axis and the polarization direction of the ionization pulse, ϕ is the corresponding azimuthal angle, and ϑ depends on θ, ϕ, and α through the coordinate transformation of $\cos\vartheta = \cos\alpha\cos\theta - \sin\alpha\sin\theta\cos\phi$.

In the second step, we calculate the population distributions in the electronic ground state and the two electronically excited $A\,^2\Pi_u$ and $B\,^2\Sigma_u^+$ states of N_2^+ after the interaction with an intense few-cycle ionization pulse by solving the TDSE for the vibrational and electronic excitations [12],

$$i\hbar\frac{\partial}{\partial t}\mathbf{\Psi}(r,t) = \left[-\frac{\hbar^2}{2\mu}\frac{\partial^2}{\partial r^2} + \mathbf{V}_0(r) + E(t)\cos\theta\mathbf{D}_{\rm XB}(r) + E(t)\sin\theta\mathbf{D}_{\rm XA}(r)\right]\mathbf{\Psi}(r,t), \quad (5)$$

where r represents the internuclear distance, μ the reduced mass of N_2^+, and $E(t)$ the electric field of the few-cycle ionization pulse. The wave function $\mathbf{\Psi}(r,t)$ is a column vector of the vibrational wave functions defined as

$$\mathbf{\Psi}(r,t) = \begin{pmatrix}\psi_X(r,t)\\ \psi_A(r,t)\\ \psi_B(r,t)\end{pmatrix}, \quad (6)$$

where $\psi_X(r,t)$, $\psi_A(r,t)$, and $\psi_B(r,t)$ represent the vibrational wave functions of the three electronic states $X\,^2\Sigma_g^+$, $A\,^2\Pi_u$, and $B\,^2\Sigma_u^+$ of N_2^+ [see Fig. 1(b)]. The 3×3 matrix $\mathbf{V}_0(r)$ is a diagonal matrix having the potential energy curves of the $X\,^2\Sigma_g^+$, $A\,^2\Pi_u$, and $B\,^2\Sigma_u^+$ states as the diagonal elements, $\mathbf{D}_{\rm XA}(r)$ is a 3×3 matrix having nonzero dipole transition matrix elements only between the $X\,^2\Sigma_g^+$ and $A\,^2\Pi_u$ states, and $\mathbf{D}_{\rm XB}(r)$ is a matrix having nonzero dipole transition matrix elements only between the $X\,^2\Sigma_g^+$ and $B\,^2\Sigma_u^+$ states. The $X\,^2\Sigma_g^+$ and $A\,^2\Pi_u$ states are coupled by a perpendicular dipole transition and the $X\,^2\Sigma_g^+$ and $B\,^2\Sigma_u^+$ states are coupled by a parallel transition. Because of the same ungerade symmetry, there is no dipole coupling between the $A\,^2\Pi_u$ and $B\,^2\Sigma_u^+$ states. The numerical values of the matrix elements for $\mathbf{V}_0$, $\mathbf{D}_{\rm XB}$, and $\mathbf{D}_{\rm XA}$ are taken from [27,28].

In solving the TDSE of Eq. (5), we define the initial conditions by assuming that N_2^+ is prepared at $t = t_0$ by the vertical ionization of N_2 in the vibrational ground $v = 0$ state of the electronic ground state, whose wave function is denoted as $\chi_0(r)$, and that the nuclear wave function of N_2^+ at $t = t_0$ takes the form of the nuclear wave function $\chi_0(r)$ of N_2. Upon the ionization, N_2^+ is prepared in either one of the three electronic states, $X\,^2\Sigma_g^+$, $A\,^2\Pi_u$, and $B\,^2\Sigma_u^+$, and their

relative yields are calculated as the θ-dependent Ammosov-Delone-Krainov (ADK) rates of tunneling ionization from the ground state of N_2 to N_2^+ [29]. The θ-dependent ADK rates for the formation of N_2^+ in the $X\,^2\Sigma_g^+$, $A\,^2\Pi_u$, and $B\,^2\Sigma_u^+$ states under the laser electric field amplitude at $t = t_0$, $E(t_0)$ (>0), are hereafter denoted as $w_X(\theta, E(t_0))$, $w_A(\theta, E(t_0))$, and $w_B(\theta, E(t_0))$, respectively.

Once the ionization is achieved at a set of given values of t_0 and θ, we solve Eq. (5) for the three cases starting from the three different electronic states of N_2. For all three electronic states, the initial vibrational wave function is assumed to be the vibrational ground-state wave function of neutral N_2 denoted as $\chi_0(r)$. After solving Eq. (5), the final wave functions in the $X\,^2\Sigma_g^+$, $A\,^2\Pi_u$, and $B\,^2\Sigma_u^+$ states are given as

$$\mathbf{\Psi}_{\text{final}\leftarrow X}(r,\theta,t_0) = \begin{pmatrix} \psi_{X\leftarrow X}(r,\theta,t_0) \\ \psi_{A\leftarrow X}(r,\theta,t_0) \\ \psi_{B\leftarrow X}(r,\theta,t_0) \end{pmatrix}, \tag{7}$$

assuming that N_2^+ is initially prepared in the $X\,^2\Sigma_g^+$ state. The final population in the $v = 0$ level of the $X\,^2\Sigma_g^+$ state whose wave function is denoted as $\chi_X(r, v = 0)$ is given as $|\langle\psi_{X\leftarrow X}(r,\theta,t_0) \mid \chi_X(r, v = 0)\rangle|^2$, and the final population in the $v = 0$ level of the $B\ ^2\Sigma_u^+$ state whose wave function is denoted as $\chi_B(r, v = 0)$ is given as $|\langle\psi_{B\leftarrow X}(r,\theta,t_0) \mid \chi_B(r, v = 0)\rangle|^2$.

Then, the population difference between the $v = 0$ level in the $B\ ^2\Sigma_u^+$ state and the $v = 0$ level in the $X\,^2\Sigma_g^+$ state is represented as

$$\begin{aligned}\Delta n_X(\theta,t_0) = {} & |\langle\psi_{B\leftarrow X}(r,\theta,t_0) \mid \chi_B(r, v = 0)\rangle|^2 \\ & - |\langle\psi_{X\leftarrow X}(r,\theta,t_0) \mid \chi_X(r, v = 0)\rangle|^2. \end{aligned} \tag{8}$$

In a similar manner as defined in Eq. (8), when N_2^+ is prepared initially in the $A\,^2\Pi_u$ state, the final population difference between the $v = 0$ level in the $B\,^2\Sigma_u^+$ state and the $v = 0$ level in the $X\,^2\Sigma_g^+$ state is denoted as $\Delta n_A(\theta,t_0)$, and when N_2^+ is prepared initially in the $B\,^2\Sigma_u^+$ state, the $B\,^2\Sigma_u^+(v = 0)$-$X\,^2\Sigma_g^+(v = 0)$ population difference is denoted as $\Delta n_B(\theta,t_0)$. Consequently, the population difference between the $v = 0$ level in the $B\,^2\Sigma_u^+$ state and the $v = 0$ level in the $X\,^2\Sigma_g^+$ state can be represented as

$$\begin{aligned}\Delta N(\theta,t_0) = {} & N_0[w_X(\theta,E(t_0))\Delta n_X(\theta,t_0) \\ & + w_A(\theta,E(t_0))\Delta n_A(\theta,t_0) \\ & + w_B(\theta,E(t_0))\Delta n_B(\theta,t_0)], \end{aligned} \tag{9}$$

where N_0 is a normalization constant. The population difference integrated over the ionization time t_0 is obtained by

$$\Delta N_{\text{int}}(\theta) = \int \Delta N(\theta,t_0)dt_0. \tag{10}$$

For a given value of the delay time τ and the angle α, the angular distribution of the direction of the N-N axis is expressed as $U(\theta,\phi;\tau,\alpha)$ given by Eq. (4), and the total population difference $\Delta N_T(\tau,\alpha)$ can be obtained by integrating the product of $U(\theta,\phi;\tau,\alpha)$ and $\Delta N_{\text{int}}(\theta)$ as

$$\Delta N_T(\tau,\alpha) = \iint U(\theta,\phi;\tau,\alpha)\Delta N_{\text{int}}(\theta)\sin\theta d\theta d\phi. \tag{11}$$

The intensity I_{lasing} of the 391-nm lasing signal is considered to be proportional to the exponential of the total τ-dependent population difference $\Delta N_T(\tau,\alpha)$ between $B\,^2\Sigma_u^+(v = 0)$ and $X\,^2\Sigma_g^+(v = 0)$ given by Eq. (11). We write $I_{\text{lasing}} = I_0 e^{q\Delta N_T(\tau,\alpha)}$, where $q = L\sigma\rho$ is a parameter depending on the length of the plasma channel $L \approx 2$ mm, the stimulated emission cross section σ, and the molecular density $\rho \approx 2 \times 10^{19}$ cm^{-3} in the plasma.

We compare the dependence of the recorded lasing intensity shown in Fig. 2 with the theoretical signal $I_{\text{lasing}} = I_0 e^{q\Delta N_T(\tau,\alpha)}$ where I_0 and $q \approx 4 \times 10^6$ are obtained by a least-square fit to the experimental signal. The theoretically obtained value for the population difference at $\tau = 1$ ps is $\Delta N_T(1\text{ ps},0) \approx 2 \times 10^{-7}$, corresponding to a population difference per volume of $\rho\Delta N_T(1\text{ ps},0) \approx 4 \times 10^{12}$ cm^{-3}, and a gain coefficient of $g \approx (q/L)\Delta N_T(1\text{ ps},0) \approx 4$ cm^{-1}. In the numerical simulation, the rotational temperature is set to be $T = 295$ K, the parameters for the alignment laser pulse are $I = 5 \times 10^{13}$ W/cm^2, $\Delta t_{\text{FWHM}} = 50$ fs, and $\lambda = 800$ nm, and those for the ionization laser pulse are $I = 4.1 \times 10^{14}$ W/cm^2, $\Delta t_{\text{FWHM}} = 5$ fs, and $\lambda = 800$ nm. As shown in Fig. 2, the result of the simulation reproduces well the recorded τ dependence of the lasing intensity at 391 nm.

In the theoretically obtained lasing signal shown in Fig. 2, very weak peak profiles can be seen at around 1.1, 3.2, 5.3, and 7.4 ps, which correspond, respectively, to 1/8, 3/8, 5/8, and 7/8 revivals of N_2. The higher-order fractional revivals originate from a partial rephasing of the rotational wave packet, which do not appear in the field-free alignment of N_2 [30] as long as the extent of the revival is represented by $\langle\cos^2\theta\rangle$. Given a rotational wave packet $|\psi(t)\rangle = \sum_j c_j e^{-itBj(j+1)/\hbar}|j,M\rangle$, where the sum runs over either odd j or even j depending on the initial state before the rotational excitation, the expectation value of $\cos^{2\ell}\theta$ can be written as

$$\begin{aligned}&\langle\psi(t)|\cos^{2\ell}\theta|\psi(t)\rangle \\ &\quad = \sum_{p=0}^{\ell}\sum_{j=0}^{\infty}(2-\delta_{p0})\text{Re}(c_j^* c_{j+2p} e^{-itB[4pj+2p(2p+1)]/\hbar}) \\ &\qquad \times\langle j,M|\cos^{2\ell}\theta|j+2p,M\rangle. \end{aligned} \tag{12}$$

A fractional revival occurs at a time t_{frac} when the phases $4tBpj/\hbar$ become equal (modulo 2π) for all values of j. The earliest fractional revival is obtained when $p = \ell$, which gives $t_{\text{frac}} = T_{\text{rot}}/(4\ell)$, expressed in terms of the rotational period T_{rot} [30]. The higher-order fractional revivals appear in the theoretically calculated ΔN_T since the distribution $\Delta N_{\text{int}}(\theta)$ defined in Eq. (10) contains higher orders of $\cos^{2\ell}\theta$. If we first expand $\Delta N_{\text{int}}(\theta)$ in even order normalized Legendre polynomials as $\Delta N_{\text{int}}(\theta) = \sum_{\ell=0}^{\infty} b_{2\ell} P_{2\ell}(\theta)$, where $b_{2\ell} = \int d\theta\ \sin\theta P_{2\ell}(\theta)\Delta N_{\text{int}}(\theta)$, and rewrite the sum in terms of $\cos^{2\ell}\theta$, we derive (up to the order of $2\ell = 6$)

$$\Delta N_{\text{int}}(\theta) \approx -0.26 + 0.14\cos^2\theta + 7.9\cos^4\theta - 8.0\cos^6\theta. \tag{13}$$

The contribution from the $\cos^4\theta$ term is responsible for the appearance of the 1/8, 3/8, 5/8, and 7/8 revivals.

Higher-order fractional revivals have previously been discussed in the context of high-harmonic generation [31,32], where the fractional revivals originate from the deviation of the θ dependence of the emission probability of the high-order harmonics from the $\cos^2\theta$ shape. Higher-order fractional revivals have also been measured in experiments on the alignment of molecules in which the alignment is monitored by fragment ions produced after molecular dissociation [33]. Our theoretical results shown in Fig. 2 demonstrate that the higher-order fractional revivals can appear in the lasing signal from aligned N_2^+ ions, originating from the $\cos^4\theta$ and $\cos^6\theta$ terms in $\Delta N_{\rm int}(\theta)$ shown in Eq. (13).

We also perform the simulation by varying the angle α and plot the resultant theoretical lasing signal $I_{\rm lasing} = I_0 e^{q\Delta N_{\rm T}(\tau,\alpha)}$ with the red solid curve as a function of α in Fig. 3 by fixing τ to be $\tau = 4.1$ ps. As shown in Fig. 3, the observed sinusoidal dependence of the lasing intensity on α is well reproduced by the simulation.

The good agreements between the experimental and theoretical lasing intensities in Figs. 2 and 3 show that the post-ionization population transfer in N_2^+ between $X\,^2\Sigma_g^+$ and $A\,^2\Pi_u$ and that between $X\,^2\Sigma_g^+$ and $B\,^2\Sigma_u^+$ induced by the few-cycle ionization pulse is a promising scenario for the population inversion resulting in the air lasing.

There are two factors that determine the variation of $\Delta N_{\rm T}$ as a function of τ (as shown in Fig. 2) and α (as shown in Fig. 3). The two factors are $\Delta n_{X,A,B}(\theta,t_0)$ and $w_{X,A,B}(\theta,E(t_0))$. In order to understand the relative contributions of these two factors, we plot $\Delta n_{X,A,B}(\theta,t_0)$ in Fig. 4(a) and $w_{X,A,B}(\theta,E(t_0))$ in Fig. 4(b) evaluated when $t_0 = 0$, that is, when the ionization occurs at the peak of the laser pulse, as a function of θ. In Fig. 4(c), we show $\Delta N(\theta,t_0)$ defined in Eq. (9), and $\Delta N_{\rm int}(\theta)$ defined in Eq. (10).

We can see in Fig. 4(a) that, when the N_2^+ ion is produced in the $X\,^2\Sigma_g^+$ state after the ionization, $\Delta n_X(\theta,t_0)$, has a peak at $\theta \approx 40^\circ$, which can be interpreted by the coexisting $A\,^2\Pi_u$-$X\,^2\Sigma_g^+$ and $B\,^2\Sigma_u^+$-$X\,^2\Sigma_g^+$ couplings [12]. When $\theta = 0^\circ$, there is no coupling between $A\,^2\Pi_u$ and $X\,^2\Sigma_g^+$, and when $\theta = 90^\circ$, there is no coupling between $B\,^2\Sigma_u^+$ and $X\,^2\Sigma_g^+$. Therefore, in order that the population transfer proceeds, the two couplings should coexist, which can be realized when θ takes the intermediate angle in the range between 0° and 90°. According to the numerical result shown in Fig. 4(a), the optimized angle for achieving the largest population difference between the $B\,^2\Sigma_u^+$ state and the $X\,^2\Sigma_g^+$ state is around 40°.

As shown in Fig. 4(b), the rate $w_X(\theta)$ of the ionization to the $X\,^2\Sigma_g^+$ state becomes maximum at $\theta = 0^\circ$ and minimum at $\theta = 90^\circ$. In the calculation of $\Delta N(\theta,t_0)$ the largest contribution to the sum comes from the $X\,^2\Sigma_g^+$ state because the ionization rate w_X is larger than w_A and w_B. At $t_0 = 0$ and $\theta = 30^\circ$, corresponding to the peak of $\Delta N(\theta,t_0)$ shown in Fig. 4(c), the relative contributions to $\Delta N(\theta,t_0)$ from the $A\,^2\Pi_u$ and $B\,^2\Sigma_u^+$ states compared to the contribution from the $X\,^2\Sigma_g^+$ state are $w_A\Delta n_A/w_X\Delta n_X \approx -0.06$ and $w_B\Delta n_B/w_X\Delta n_X \approx 0.2$. As shown in Fig. 4(c), $\Delta N_{\rm int}(\theta)$, which includes the contributions from all ionization times, also exhibits a peak at $\theta \approx 30^\circ$,

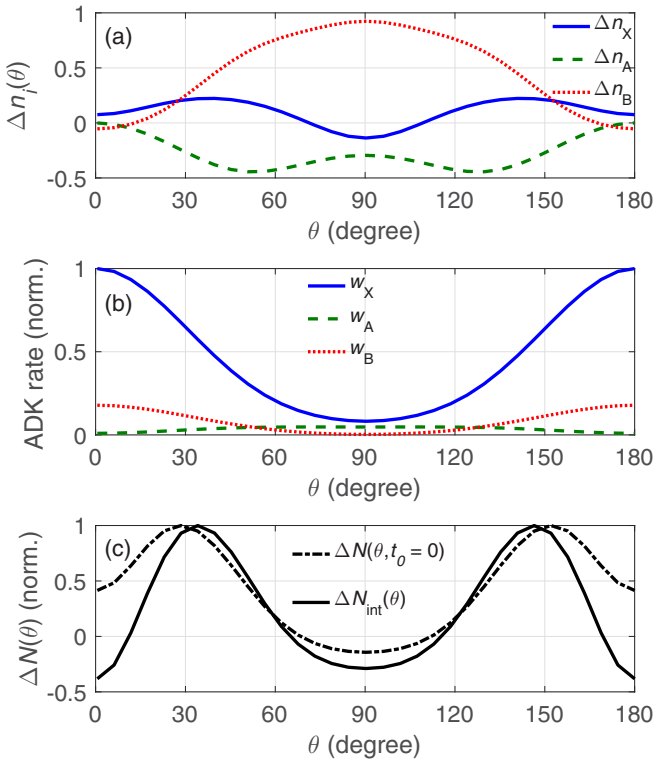

FIG. 4. (a) Final population difference $\Delta n_i(\theta,t_0)$, for N_2^+ ion prepared in the state i after the ionization at time $t_0 = 0$. (b) ADK rate normalized so that $w_X(\theta = 0) = 1$. (c) $\Delta N(\theta,t_0)$ and $\Delta N_{\rm int}(\theta)$ (normalized). The field intensity is $I = 4.1 \times 10^{14}$ W/cm^2.

which confirms that the dominant contribution to the integrated population difference $\Delta N_{\rm int}(\theta)$ originates from the ionization times around $t_0 = 0$ for the ionization to the $X\,^2\Sigma_g^+$ state of N_2^+. In the Supplemental Material [34], the variation of $\Delta N_{\rm T}(\tau,\alpha)$ at different τ values is discussed on the basis of Eq. (11).

In summary, by preparing the rotational wave packet of N_2 by an alignment pulse, we have shown that the N_2^+ lasing emission at 391 nm exhibits not only a characteristic rotational recurrence pattern as a function of the delay time τ but also a strong modulation as a function of the polarization angle difference α. The experimental results have been well reproduced numerically by the combined model of the light-field-induced coupling of N_2^+ with the time-dependent rotational motion of N_2, which strongly supports the post-ionization population transfer by the $B\,^2\Sigma_u^+$-$X\,^2\Sigma_g^+$ and $A\,^2\Pi_u$-$X\,^2\Sigma_g^+$ electronic state couplings proposed in [12] as the mechanism of air lasing in N_2^+.

The work is supported in part by the National Natural Science Foundation of China (61625501, 61427816, 61235003); the National Basic Research Program of China (2014CB921300); the Ministry of Education, Culture, Sports, Science and Technology (MEXT), Japan; the Grant-in-Aid for Specially Promoted Research (Grants No. 19002006 and No. 15H05696); the Grant-in-Aid for Scientific Research A (Grant No. 24245003); and a Grant-in-Aid for Young Scientists B (Grant No. 15K17805).

[1] Q. Luo, W. Liu, and S. L. Chin, Lasing action in air induced by ultra-fast laser filamentation, Appl. Phys. B **76**, 337 (2003).

[2] A. Dogariu, J. B. Michael, M. O. Scully, and R. B. Miles, High-gain backward lasing in air, Science **331**, 442 (2011).

[3] D. Kartashov, S. Alisauskas, A. Baltuska, A. Schmitt-Sody, W. Roach, and P. Polynkin, Remotely pumped stimulated emission at 337 nm in atmospheric nitrogen, Phys. Rev. A **88**, 041805(R) (2013).

[4] S. Mitryukovskiy, Y. Liu, P. Ding, A. Houard, and A. Mysyrowicz, Backward stimulated radiation from filaments in nitrogen gas and air pumped by circularly polarized 800 nm femtosecond laser pulses, Opt. Express **22**, 12750 (2014).

[5] A. Laurain, M. Scheller, and P. Polynkin, Low-Threshold Bidirectional Air Lasing, Phys. Rev. Lett. **113**, 253901 (2014).

[6] J. Yao, H. Xie, B. Zeng, W. Chu, G. Li, J. Ni, H. Zhang, C. Jing, C. Zhang, H. Xu, Y. Cheng, and Z. Xu, Gain dynamics of a free-space nitrogen laser pumped by circularly polarized femtosecond laser pulses, Opt. Express **22**, 19005 (2014).

[7] J. Yao, B. Zeng, H. L. Xu, G. Li, W. Chu, J. Ni, H. Zhang, S. L. Chin, Y. Cheng, and Z. Z. Xu, High-brightness switchable multiwavelength remote laser in air, Phys. Rev. A **84**, 051802(R) (2011).

[8] G. Point, Y. Liu, Y. Brelet, S. Mitryukovskiy, P. Ding, A. Houard, and A. Mysyrowicz, Lasing of ambient air with microjoule pulse energy pumped by a multi-terawatt infrared femtosecond laser, Opt. Lett. **39**, 1725 (2014).

[9] G. Li, C. Jing, B. Zeng, H. Xie, J. Yao, W. Chu, J. Ni, H. Zhang, H. L. Xu, Y. Cheng, and Z. Z. Xu, Signature of superradiance from a nitrogen gas plasma channel produced by strong field ionization, Phys. Rev. A **89**, 033833 (2014).

[10] J. Ni, W. Chu, C. Jing, H. Zhang, B. Zeng, J. Yao, G. Li, H. Xie, C. Zhang, H. Xu, S. L. Chin, Y. Cheng, and Z. Xu, Identification of the physical mechanism of generation of coherent N_2^+ emissions in air by femtosecond laser excitation. Opt. Express **21**, 8746 (2013).

[11] M. Lei, C. Wu, A. Zhang, Q. Gong, and H. Jiang, Population inversion in the rotational levels of the superradiant N_2^+ pumped by femtosecond laser pulses, Opt. Express. **25**, 4535 (2017).

[12] H. Xu, E. Lötstedt, A. Iwasaki, and K. Yamanouchi, Sub-10-fs population inversion in N_2^+ in air lasing through multiple state coupling, Nat. Commun. **6**, 8347 (2015).

[13] H. S. Zhang, C. Jing, J. Yao, G. Li, B. Zeng, W. Chu, J. Ni, H. Xie, H. L. Xu, S. L. Chin, K. Yamanouchi, Y. Cheng, and Z. Z. Xu, Rotational Coherence Encoded in an "Air-Laser" Spectrum of Nitrogen Molecular Ions in an Intense Laser Field, Phys. Rev. X **3**, 041009 (2013).

[14] J. Ni, W. Chu, H. Zhang, B. Zeng, J. Yao, L. Qiao, G. Li, C. Jing, H. Xie, H. L. Xu, Y. Cheng, and Z. Z. Xu, Impulsive rotational Raman scattering of N_2 by a remote "air laser" in femtosecond laser filament. Opt. Lett. **39**, 2250 (2014).

[15] D. Kartashov, S. Alisauskas, G. Andriukaitis, A. Pugzlys, S. Haessler, A. Baltuska, M. Shneider, B. Landgraf, A. Hoffmann, C. Spielmann, P. G. Polynkin, A. Mitrofanov, D. Sidorov-Biryukov, A. Zheltikov, J. Möhring, D. Starukhin, M. Motzkus, M. Ivanov, M. Richter, and F. Morales, *Standoff Sources of Coherent Radiation Initiated by Femtosecond Filaments*, in CLEO: 2015, OSA Technical Digest (online) (Optical Society of America, Washington, DC, 2015), Paper SM2N. 3.

[16] Y. Liu, P. Ding, G. Lambert, A. Houard, V. Tikhonchuk, and A. Mysyrowicz, Recollision-Induced Superradiance of Ionized Nitrogen Molecules, Phys. Rev. Lett. **115**, 133203 (2015).

[17] J. Yao, S. Jiang, W. Chu, B. Zeng, C. Wu, R. Lu, Z. Li, H. Xie, G. Li, C. Yu, Z. Wang, H. Jiang, Q. Gong, and Y. Cheng, Population Redistribution Among Multiple Electronic States of Molecular Nitrogen Ions in Strong Laser Fields, Phys. Rev. Lett. **116**, 143007 (2016).

[18] H. Xu, Y. Cheng, S. L. Chin, and H. B. Sun, Femtosecond laser ionization and fragmentation of molecules for environmental sensing, Laser Photon. Rev. **9**, 275 (2015).

[19] Fiber spectrometer from Ocean Optics USB4000-UV-VIS.

[20] H. Cai, J. Wu, A. Couairon, and H. Zeng, Spectral modulation of femtosecond laser pulse induced by molecular alignment revivals, Opt. Lett. **34**, 827 (2009).

[21] J. Wu, H. Cai, A. Couairon, and H. Zeng, Wavelength tuning of a few-cycle laser pulse by molecular alignment in femtosecond filamentation wake, Phys. Rev. A **79**, 063812 (2009).

[22] J. Wu, H. Cai, Y. Peng, Y. Tong, A. Couairon, and H. Zeng, Control of femtosecond filamentation by field-free revivals of molecular alignment, Laser Phys. **19**, 1759 (2009).

[23] J. Wu, H. Cai, A. Couairon, and H. Zeng, Few-cycle shock X-wave generation by filamentation in prealigned molecules, Phys. Rev. A **80**, 013828 (2009).

[24] H. Stapelfeldt and T. Seideman, Colloquium: Aligning molecules with strong laser pulses, Rev. Mod. Phys. **75**, 543 (2003).

[25] D. Spelsberg and W. Meyer, Dynamic multipole polarizabilities, reduced spectra, and interaction coefficients for N_2 and CO, J. Chem. Phys. **111**, 9618 (1999).

[26] A. Lofthus and P. H. Krupenie, The spectrum of molecular nitrogen, J. Phys. Chem. Ref. Data **6**, 113 (1977).

[27] S. R. Langhoff, C. W. Bauschlicher, Jr., and H. Partridge, Theoretical study of the N_2^+ Meinel system, J. Chem. Phys. **87**, 4716 (1987).

[28] S. R. Langhoff and C. W. Bauschlicher, Jr., Theoretical study of the first and second negative systems of N_2^+, J. Chem. Phys. **88**, 329 (1988).

[29] S. F. Zhao, J. Cheng, A. T. Le, T. F. Jiang, and C. D. Lin, Determination of structure parameters in strong-field tunneling ionization theory of molecules, Phys. Rev. A **81**, 033423 (2010).

[30] A. Abdurrouf and F. H. M. Faisal, Theory of intense-field dynamic alignment and high-order harmonic generation from coherently rotating molecules and interpretation of intense-field ultrafast pump-probe experiments, Phys. Rev. A **79**, 023405 (2009).

[31] T. Kanai, S. Minemoto, and H. Sakai, Quantum interference during high-order harmonic generation from aligned molecules, Nature (London) **435**, 470 (2005).

[32] R. M. Lock, S. Ramakrishna, X. Zhou, H. C. Kapteyn, M. M. Murnane, and T. Seideman, Extracting Continuum Electron Dynamics from High Harmonic Emission from Molecules, Phys. Rev. Lett. **108**, 133901 (2012).

[33] S. J. Weber, M. Oppermann, and J. P. Marangos, Role of Rotational Wave Packets in Strong Field Experiments, Phys. Rev. Lett. **111**, 263601 (2013).

[34] See Supplemental Material at http://link.aps.org/supplemental/10.1103/PhysRevA.96.041401 for the analysis of the τ dependence of the total population difference.